

Hydrogen motion and site occupation in $\text{Ti}_2\text{CoH}_x(\text{D}_x)$: NMR and neutron scattering studies

A.V. Skripov^{a,*}, A.L. Buzlukov^a, A.V. Soloninin^a, V.I. Voronin^a,
I.F. Berger^b, T.J. Udovic^c, Q. Huang^c, J.J. Rush^c

^a*Institute of Metal Physics, Urals Branch of the Academy of Sciences, Ekaterinburg 620041, Russia*

^b*Institute of Solid State Chemistry, Urals Branch of the Academy of Sciences, Ekaterinburg 620041, Russia*

^c*NIST Center for Neutron Research, National Institute of Standards and Technology, Gaithersburg, MD 20899, USA*

Received 14 June 2006; received in revised form 15 September 2006; accepted 5 December 2006

Abstract

Nuclear magnetic resonance measurements of the ^1H and ^2D spin–lattice relaxation rates R_1 for Ti_2Ni -type compounds $\text{Ti}_2\text{CoH}_{0.5}$, $\text{Ti}_2\text{CoH}_{0.9}$ and $\text{Ti}_2\text{CoD}_{1.0}$ have been combined with inelastic neutron scattering (INS) measurements of the H(D) vibrational spectra and neutron diffraction measurements for the same samples. The R_1 results for $\text{Ti}_2\text{CoH}_{0.9}$ and $\text{Ti}_2\text{CoD}_{1.0}$ give evidence for the existence of a fast H(D) motion with the characteristic jump rate of about $3 \times 10^8 \text{ s}^{-1}$ at room temperature, whereas for $\text{Ti}_2\text{CoH}_{0.5}$ such a fast motional process is absent. The results of the INS and neutron diffraction measurements suggest that the appearance of the fast hydrogen jump process in $\text{Ti}_2\text{CoH}_x(\text{D}_x)$ with $x \approx 1$ is related to the occupation of an additional type of interstitial sites by hydrogen atoms. While in $\text{Ti}_2\text{CoH}_{0.5}$, hydrogen atoms are found to occupy only the octahedral sites with Ti_6 coordination, a partial occupation of the tetrahedral Ti_3Co and Ti_2Co_2 sites by H(D) atoms (in addition to the nearly completely filled sublattice of the octahedral sites) has been revealed for $\text{Ti}_2\text{CoH}_{0.9}$ and $\text{Ti}_2\text{CoD}_{1.0}$. Possible paths of hydrogen jump motion in $\text{Ti}_2\text{CoH}_x(\text{D}_x)$ are discussed on the basis of the distances between the sites partially occupied by H(D) atoms.

© 2007 Elsevier B.V. All rights reserved.

PACS: 66.30.–h; 76.60.Es; 78.70.Nx; 61.12.Ld

Keywords: Metal–hydrogen systems; Hydrogen diffusion; Nuclear magnetic resonance; Neutron scattering

1. Introduction

Intermetallic compounds A_2B with the cubic Ti_2Ni -type structure can absorb large amounts of hydrogen [1–3]. Some of these compounds retain the host-lattice structure up to the maximum attainable hydrogen content forming solid solutions A_2BH_x ($x \leq 5$) [3]. These features make Ti_2Ni -type compounds attractive for hydrogen-storage applications as well as for studies of the effects of hydrogen absorption on the physical properties of intermetallics. However, the available information on the properties of the hydrogen sublattice (including the positions and mobility of H atoms) in Ti_2Ni -type compounds is still

fragmentary. While hydrogen diffusion in most of the studied Ti_2Ni -type intermetallics [4–7] is found to be rather slow, recent proton nuclear magnetic resonance (NMR) measurements [8] have revealed a fast H jump process in Ti_2Ni -type $\text{Ti}_2\text{CoH}_{1.34}$ with the characteristic jump rate $\tau_1^{-1} \approx 3 \times 10^8 \text{ s}^{-1}$ at room temperature. This process coexists with much slower H motion having the characteristic jump rate $\tau_2^{-1} \approx 2 \times 10^5 \text{ s}^{-1}$ at room temperature [8].

The main results of Ref. [8] are reproduced in Fig. 1 showing the temperature dependence of the proton spin–lattice relaxation rate R_1 for $\text{Ti}_2\text{CoH}_{1.34}$ measured at the NMR frequencies $\omega/2\pi = 13, 23.8$ and 40 MHz. Each of the two frequency-dependent $R_1(T)$ peaks should occur at the temperature at which the hydrogen jump rate τ_i^{-1} becomes nearly equal to ω [9]; therefore, the faster jump process (with the jump rate τ_1^{-1}) gives rise to the

*Corresponding author.

E-mail address: skripov@imp.uran.ru (A.V. Skripov).

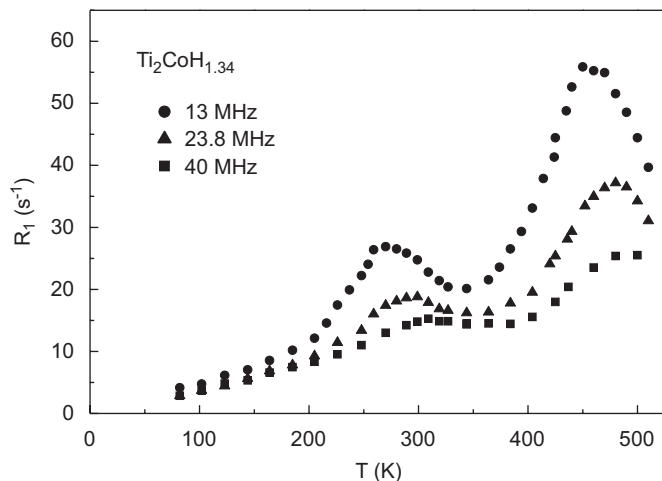


Fig. 1. The temperature dependence of the proton spin–lattice relaxation rate for $\text{Ti}_2\text{CoH}_{1.34}$ measured at 13, 23.8 and 40 MHz (from Ref. [8]).

low-temperature R_1 peak, while the slower jump process (with the jump rate $\tau_2^{-1} \ll \tau_1^{-1}$) is responsible for the high-temperature R_1 peak. However, at lower H content in Ti_2CoH_x ($x = 0.56$) the low-temperature R_1 peak, and thus the fast jump process, is absent [8]. In order to elucidate the origin of the changes in H mobility in Ti_2CoH_x over the range of x from 0.56 to 1.34, in the present work we have studied the H(D) motion and site occupation in $\text{Ti}_2\text{CoH}_x(\text{D}_x)$ at low and intermediate H(D) concentrations ($0.5 \leq x \leq 1.0$) using NMR and neutron scattering techniques. NMR measurements of the ^1H and ^2D spin–lattice relaxation rates, inelastic neutron scattering (INS) measurements of the H(D) vibrational spectra and neutron diffraction measurements are combined to demonstrate that the appearance of the fast hydrogen jump process in $\text{Ti}_2\text{CoH}_x(\text{D}_x)$ is related to the occupation of an additional type of interstitial sites by hydrogen atoms.

2. Experimental details

The intermetallic compound Ti_2Co was prepared by arc melting the appropriate amounts of high-purity Ti and Co in a helium atmosphere followed by an annealing in vacuum at 1200 K for 50 h. According to X-ray diffraction analysis, the annealed sample contained the dominant Ti_2Ni -type phase with the lattice parameter $a = 11.295 \text{ \AA}$ and a small amount ($\sim 2 \text{ wt\%}$) of TiCo with CsCl-type structure and $a = 2.997 \text{ \AA}$. Small pieces of Ti_2Co were charged with hydrogen at a pressure of about 1 bar using a Sieverts-type vacuum system. After annealing the intermetallic in vacuum at 973 K, the system was cooled down to 853 K, and H_2 (or D_2) gas was admitted into the system at this temperature. The amount of absorbed hydrogen was determined from the pressure change in the calibrated volume of the system after slowly cooling down to room temperature. NMR and neutron scattering measurements were made on the hydrided samples $\text{Ti}_2\text{CoH}_{0.5}$, $\text{Ti}_2\text{CoH}_{0.9}$ and $\text{Ti}_2\text{CoD}_{1.0}$. According to X-ray diffraction analysis,

the dominant phase in these samples retains the Ti_2Ni -type host–lattice structure with the lattice parameters $a = 11.333 \text{ \AA}$ ($\text{Ti}_2\text{CoH}_{0.5}$), 11.362 \AA ($\text{Ti}_2\text{CoH}_{0.9}$) and 11.363 \AA ($\text{Ti}_2\text{CoD}_{1.0}$). The minor phase ($\sim 2\text{--}7 \text{ wt\%}$) with CsCl-type structure in all these samples has the same lattice parameter as in the hydrogen-free sample; this indicates that the minor phase does not absorb hydrogen under the experimental conditions described above.

Measurements of the nuclear spin–lattice relaxation rates R_1 were performed on a modernized Bruker SXP pulse NMR spectrometer at the frequencies $\omega/2\pi = 13.8 \text{ MHz}$ (^2D), 23.8 and 90 MHz (^1H) using the saturation–recovery method. INS measurements of the H(D) vibrational spectra were performed on the filter-analyzer neutron spectrometer (FANS) [10] at the NIST Center for Neutron Research. The vibrational spectra of H and D were measured using the Cu (220) monochromator and horizontal collimations of $20'$ of arc before and after the monochromator (for H) and $60'$ and $20'$ of arc, respectively (for D). Neutron diffraction measurements at room temperature were performed on the powder diffractometer D7a [11] at the research reactor IVV-2 M of the Institute of Metal Physics, Urals Branch of the Russian Academy of Sciences in Zarechnyi (for Ti_2Co , $\text{Ti}_2\text{CoH}_{0.5}$ and $\text{Ti}_2\text{CoH}_{0.9}$) and on the high-resolution powder diffractometer BT1 [12] at the NIST Center for Neutron Research (for $\text{Ti}_2\text{CoD}_{1.0}$). Powdered samples were sealed in cylindrical vanadium containers with diameters of 6 mm (D7a) and 9.2 mm (BT1). The D7a diffractometer used the double graphite (002)–Ge (511) monochromator; the neutron wavelength λ was 1.5321 \AA . The BT1 diffractometer used the Cu (311) monochromator, $\lambda = 1.5403 \text{ \AA}$. Neutron diffraction patterns were recorded in the scattering angle ranges $10^\circ \leq 2\theta \leq 133.5^\circ$ (D7a) and $3^\circ \leq 2\theta \leq 160^\circ$ (BT1) with a step of 0.05° (except for Ti_2Co for which the step was 0.1°).

Profile refinements of the diffraction patterns were made by Rietveld analysis using the FULLPROF program [13]. The neutron scattering lengths were taken from the FULLPROF library. Pseudo-Voigt profile functions were used. The background was modeled by interpolation between manually chosen points.

3. Results and discussion

3.1. Nuclear spin–lattice relaxation

The results of the proton spin–lattice relaxation rate measurements at 23.8 MHz for $\text{Ti}_2\text{CoH}_{0.5}$ and $\text{Ti}_2\text{CoH}_{0.9}$ are compared to those for $\text{Ti}_2\text{CoH}_{1.34}$ in Fig. 2. It can be seen that for $\text{Ti}_2\text{CoH}_{0.5}$, the temperature dependence of R_1 does not exhibit any peak in the range 80–400 K. In this range, the proton spin–lattice relaxation rate for $\text{Ti}_2\text{CoH}_{0.5}$ is dominated by the Korringa contribution [9] R_{1e} due to the interaction between nuclear spins and conduction electrons. The Korringa contribution is usually proportional to the temperature, $R_{1e} = C_e T$. The value of C_e

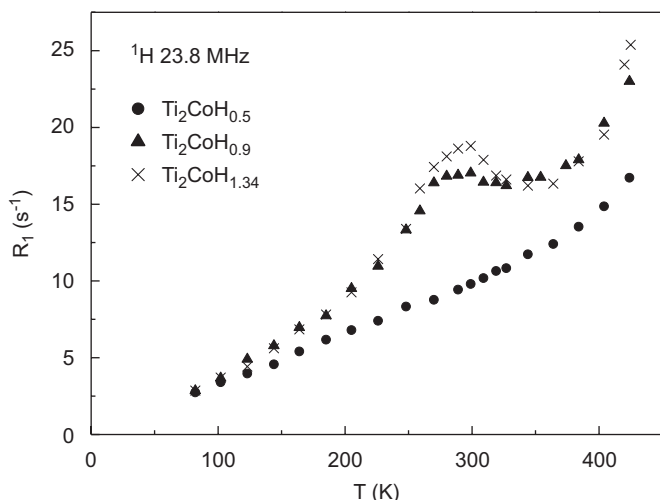


Fig. 2. The temperature dependence of the proton spin–lattice relaxation rates for $\text{Ti}_2\text{CoH}_{0.5}$, $\text{Ti}_2\text{CoH}_{0.9}$ and $\text{Ti}_2\text{CoH}_{1.34}$ at 23.8 MHz.

estimated from the experimental data for $\text{Ti}_2\text{CoH}_{0.5}$ is $3.3 \times 10^{-2} \text{ s}^{-1} \text{ K}^{-1}$. For $\text{Ti}_2\text{CoH}_{0.9}$ the temperature dependence of R_1 shows a small peak near 290 K. As can be seen from Fig. 2, the position of this peak is nearly the same as in $\text{Ti}_2\text{CoH}_{1.34}$, while the amplitude of the peak is somewhat lower. The behavior of the proton spin–lattice relaxation rate for $\text{Ti}_2\text{CoH}_{0.9}$ indicates that, in addition to the Korringa contribution, in the temperature range 200–370 K there is a considerable contribution to R_1 due to internuclear dipole–dipole interaction modulated by H motion. This motional contribution R_{1m} passes through a maximum at the temperature at which the hydrogen jump rate becomes nearly equal to the NMR frequency ($\omega\tau_i \approx 1$) and vanishes in the limits of fast ($\omega\tau_i \ll 1$) and slow ($\omega\tau_i \gg 1$) motion [9].

The amplitude of the R_{1m} peak is determined by a part of internuclear dipole–dipole interactions which is averaged out by a particular type of H motion. The long-range diffusion of hydrogen leads to complete averaging out of H–H and H–metal dipolar interactions. On the other hand, a localized jump motion of hydrogen [14–17] leads to a partial averaging of dipolar interactions; therefore, the amplitude of the R_{1m} peak originating from localized H motion is usually smaller than that originating from long-range H diffusion. On the basis of these considerations and the experimental R_1 results for a number of metal–hydrogen systems showing two frequency scales of H jump motion [14,15,18,19], we assume that the R_1 peak in Ti_2CoH_x near 290 K originates from some kind of localized H motion. Usually only a certain fraction p of H atoms participates in the fast localized motion [14,16,17]. While two coexisting fractions of H atoms with different mobilities are expected to give rise to two-exponential spin–lattice relaxation, the recovery of the ^1H nuclear magnetization in Ti_2CoH_x remains single-exponential over the entire temperature range studied. The single-exponential behavior of the proton R_1 has also been reported for

other metal–hydrogen systems showing localized H motion [14,15,18,19]. As has been demonstrated for the localized H motion in $\alpha\text{-ScH}_x$ [14], a single value of the proton spin–lattice relaxation rate can result from the rapid transfer of nuclear polarization due to mutual spin-exchange process (*spin diffusion*). This process is effective if the interacting nuclear spins have the same resonance frequencies (as expected to be true for protons in Ti_2CoH_x). In this case, the amplitude of the R_{1m} peak should be proportional to p . Because of the small amplitude of the R_{1m} peak for $\text{Ti}_2\text{CoH}_{0.9}$, we have not tried to derive the temperature dependence of τ_1^{-1} for this compound from fits to the relaxation rate data. Since the positions of the low-temperature relaxation rate peak in $\text{Ti}_2\text{CoH}_{0.9}$ and $\text{Ti}_2\text{CoH}_{1.34}$ are nearly the same (Fig. 2), it may be expected that the motional parameters of hydrogen in $\text{Ti}_2\text{CoH}_{0.9}$ are close to those found for $\text{Ti}_2\text{CoH}_{1.34}$ [8].

Fig. 3 shows the temperature dependence of the ^2D spin–lattice relaxation rate in $\text{Ti}_2\text{CoD}_{1.0}$. This temperature dependence exhibits a peak at $T \approx 290$ K, i.e., at approximately the same temperature as the ^1H relaxation rate peak in $\text{Ti}_2\text{CoH}_{0.9}$. Thus, the hydrogen jump rate for the fast motional process does not show any considerable isotope effect. However, the relaxation rate peak for ^2D appears to be much more pronounced than that for ^1H . This may be explained by a combined effect of two factors. (1) The Korringa contribution to the spin–lattice relaxation rate, R_{1e} , for ^2D is much smaller than that for ^1H . Since R_{1e} is proportional to the square of the nuclear gyromagnetic ratio γ , the Korringa contribution for ^2D should be a factor of $(\gamma_{\text{H}}/\gamma_{\text{D}})^2 = 42.4$ smaller. Therefore, the monotonic background contribution to $R_1(T)$ for ^2D is small, as compared to that for ^1H . (2) Since, in contrast to protons, ^2D nuclei have a nonzero electric quadrupole moment, there is an additional contribution to R_{1m} for deuterium

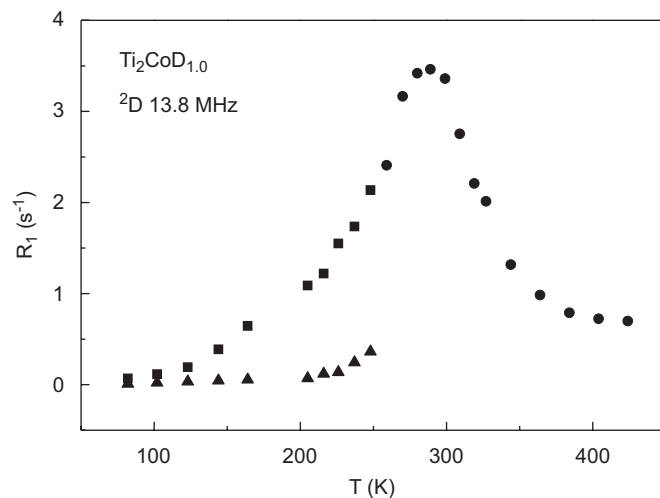


Fig. 3. The temperature dependence of the ^2D spin–lattice relaxation rate for $\text{Ti}_2\text{CoD}_{1.0}$ measured at 13.8 MHz. In the region of single-exponential relaxation the data points are shown by circles. In the region of two-exponential relaxation both the fast (squares) and slow (triangles) components of the relaxation rate are shown.

resulting from the interaction of nuclear quadrupole moments with local electric field gradients (EFG) modulated by D motion. In our case, the quadrupole contribution to R_{1m} is the dominant one, and the amplitude of the $R_{1m}(T)$ peak for ^2D appears to be considerably higher than that expected for dipole–dipole interactions.

Below $T \approx 250$ K the recovery of the ^2D nuclear magnetization is found to become two-exponential. Fig. 3 shows the behavior of both the fast and slow components of the relaxation rate. The ratio of the fast and slow relaxation rates at the same temperature appears to be considerable (for example, at 205 K this ratio is 15). Similar deviations from a single-exponential recovery below a certain temperature have been found for ^2D spin–lattice relaxation in Laves-phase systems TaV_2D_x and HfMo_2D_x [20] showing two frequency scales of D motion. It should be noted that for ^2D nuclei with the spin $I = 1$, the quadrupole relaxation is expected to be single-exponential even in the case of slow motion [21]. We can also exclude the possibility of phase separation in $\text{Ti}_2\text{CoD}_{1.0}$ at low temperatures (see Section 3.2). Therefore, as in the case of TaV_2D_x and HfMo_2D_x [20], the observed two-exponential relaxation may be ascribed to a coexistence of two fractions of D atoms with different low-temperature mobilities within a single phase. In contrast to ^1H , the spin diffusion for ^2D should be suppressed, since the nearest-neighbor ^2D nuclei have different resonance frequencies. The reason is that for the tetrahedral sites in Ti_2Co the direction of the principal axis of the EFG tensor changes from site to site, while for the octahedral sites the EFG is expected to be close to zero. Therefore, nuclear spins with different relaxation rates can contribute separately to the recovery of nuclear magnetization. The fast relaxation rate component can be attributed to the fraction of D atoms participating in the fast localized motion with the jump rate τ_1^{-1} . The dominant relaxation mechanism for this component is related to strong EFG fluctuations that occur when a deuterium atom jumps from one site to another. The slow relaxation rate component can be ascribed to the fraction of D atoms that do not participate in the fast localized motion; this component is determined by the contributions due to conduction electrons and due to the weak EFG fluctuations resulting from the motion of other (mobile) D atoms. As the temperature increases, the long-range diffusion of deuterium becomes fast enough to ‘mix’ the contributions of the two fractions of D to the recovery of nuclear magnetization, so that the recovery becomes single-exponential. It may be expected that this occurs when the slower jump rate τ_2^{-1} becomes comparable either to the difference between the resonance frequencies of ^2D in the nearest-neighbor sites or to the relaxation rate itself.

Thus, the measurements of the ^1H and ^2D spin–lattice relaxation rates in $\text{Ti}_2\text{CoH}_{0.5}$, $\text{Ti}_2\text{CoH}_{0.9}$ and $\text{Ti}_2\text{CoD}_{1.0}$ show the onset of the fast motional process as the hydrogen concentration changes from 0.5 to 0.9 atoms/formula unit, with the characteristic H(D) jump rate $\tau_1^{-1} \approx 3 \times 10^8 \text{ s}^{-1}$ at 300 K. Comparison of the data for $\text{Ti}_2\text{CoH}_{0.9}$ and

$\text{Ti}_2\text{CoD}_{1.0}$ has not revealed any considerable isotope effect on τ_1^{-1} . The spin–lattice relaxation results suggest that only a fraction of all H(D) atoms participates in the fast motional process.

3.2. Neutron vibrational spectra

The experimental low-temperature INS spectra for $\text{Ti}_2\text{CoH}_{0.5}$ and $\text{Ti}_2\text{CoH}_{0.9}$ in the energy transfer range 40–190 meV are shown in Fig. 4(a). In this energy range, the observed INS spectra are dominated by the fundamental modes of H optical vibrations. As can be seen from Fig. 4(a), the vibrational spectrum of hydrogen in $\text{Ti}_2\text{CoH}_{0.5}$ consists of a broad asymmetric peak centered near 100 meV. For $\text{Ti}_2\text{CoH}_{0.9}$ this peak is broadened, and two additional peaks appear near 137 and 157 meV. These results indicate that, in addition to the interstitial sites occupied in $\text{Ti}_2\text{CoH}_{0.5}$, hydrogen atoms in $\text{Ti}_2\text{CoH}_{0.9}$ also occupy extra sites with a different coordination and higher vibrational energies.

Fig. 4(b) shows the experimental low-temperature INS spectrum for $\text{Ti}_2\text{CoD}_{1.0}$ in the energy transfer range 40–126 meV. Since the ratio of masses of D and H is 2, in the harmonic approximation the vibrational spectrum of D should be shifted to a factor of $\sqrt{2}$ lower energies from

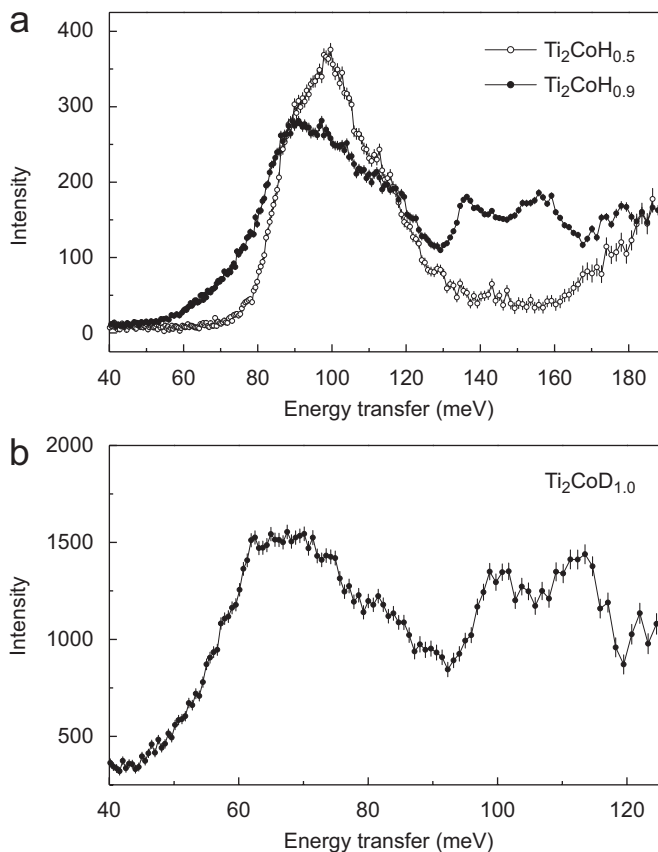


Fig. 4. The inelastic neutron scattering spectra for $\text{Ti}_2\text{CoH}_{0.5}$ and $\text{Ti}_2\text{CoH}_{0.9}$ (a) and for $\text{Ti}_2\text{CoD}_{1.0}$ (b) at 10 K. The lines through the points are only guides to the eye.

that of H. Comparison of the results for $\text{Ti}_2\text{CoH}_{0.9}$ and $\text{Ti}_2\text{CoD}_{1.0}$ (Figs. 4(a) and (b)) shows that the general features of the shape of the vibrational spectra of H and D are the same. The low-energy peak in the spectrum for $\text{Ti}_2\text{CoD}_{1.0}$ appears at a factor of $\sqrt{2}$ lower energy than the corresponding peak for $\text{Ti}_2\text{CoH}_{0.9}$, as expected. Both high-energy peaks in the spectrum for $\text{Ti}_2\text{CoD}_{1.0}$ appear at slightly ($\sim 3\%$) higher energies than those expected on the basis of the results for $\text{Ti}_2\text{CoH}_{0.9}$ in the harmonic approximation. This suggests some anharmonicity of the H(D) vibrations responsible for the high-energy peaks. It should also be noted that the relative intensity of the high-energy peaks for $\text{Ti}_2\text{CoD}_{1.0}$ is larger than that for $\text{Ti}_2\text{CoH}_{0.9}$. In addition to the low-temperature results, the INS spectrum for $\text{Ti}_2\text{CoD}_{1.0}$ has also been measured at room temperature. All the features of the room-temperature spectrum are found to be the same as those for the low-temperature spectrum. This result allows us to exclude the possibility of phase separation between 300 and 10 K.

The unit cell of a Ti_2Ni -type compound contains 456 tetrahedral interstices of 6 different types: $32e_1$ (Ti_3Ni), $192i$ (Ti_3Ni), $96g_1$ (Ti_3Ni), $96g_2$ (Ti_2Ni_2), $32e_2$ (TiNi_3) and $8b$ (Ni_4), and 24 octahedral interstices of two different types: $8a$ (Ti_6) and $16c$ (Ti_6) [22]. The volume of the octahedral holes is considerably larger than that of the tetrahedral holes [22]. Taking into account that the octahedral sites are coordinated by 6 Ti atoms with strong affinity for hydrogen, one may expect that the octahedral sites are preferably filled with hydrogen, at least at low H concentrations (the complete filling of a and c sites corresponds to $x = 0.75$). Since the nearest-neighbor H–Ti distances for H atoms in the octahedral sites of Ti_2CoH_x are rather large (~ 2.15 Å for both a and c sites), the vibrational energies of hydrogen in these sites should be lower than in the tetrahedrally coordinated sites. Therefore, we can attribute the low-energy peak in the INS spectra of $\text{Ti}_2\text{CoH}_x(\text{D}_x)$ to H(D) vibrations in the octahedral sites. The two high-energy peaks appearing in the INS spectra of $\text{Ti}_2\text{CoH}_{0.9}$ and $\text{Ti}_2\text{CoD}_{1.0}$ can be ascribed to H(D) vibrations in the smaller tetrahedral interstices, likely in Ti-rich sites. Since the point symmetry of the tetrahedral sites is lower than cubic, the split high-energy peaks appear to be quite natural. This feature originates from different bonding in different directions. The relative occupancy of the tetrahedral and octahedral sites can be roughly estimated from the relative integrated intensities of the high-energy and low-energy peaks. Ignoring the effect of the Debye–Waller factor and a possible overlap of the peaks and correcting for the contribution of the second-order vibrational peak (which is evident in the spectrum for $\text{Ti}_2\text{CoH}_{0.5}$ above 160 meV, see Fig. 4(a)), we obtain the following estimates of the fraction of H(D) atoms in the tetrahedral sites: 0.32 for $\text{Ti}_2\text{CoH}_{0.9}$ and 0.37 for $\text{Ti}_2\text{CoD}_{1.0}$. It is natural to conclude that the partial filling of some additional (tetrahedral) sites in $\text{Ti}_2\text{CoH}_{0.9}$ and $\text{Ti}_2\text{CoD}_{1.0}$ leads to the onset of the fast

H(D) motional process (giving rise to the R_1 peak near 290 K).

3.3. Neutron diffraction

The neutron diffraction patterns and the agreement between the observed and calculated intensities for Ti_2Co , $\text{Ti}_2\text{CoH}_{0.5}$, $\text{Ti}_2\text{CoH}_{0.9}$ and $\text{Ti}_2\text{CoD}_{1.0}$ are shown in Figs. 5–8. The high background intensity observed for $\text{Ti}_2\text{CoH}_{0.5}$ and $\text{Ti}_2\text{CoH}_{0.9}$ (Figs. 6 and 7) originates from the incoherent neutron scattering from protons. For all the samples studied, the dominant phase is found to have the cubic Ti_2Ni -type structure (space group $\text{Fd}\bar{3}\text{m}$) with Ti atoms in $48f$ ($x, 1/8, 1/8$) and in $16d$ ($1/2, 1/2, 1/2$) and Co atoms in $32e$ (x, x, x). The lattice parameter of this phase shows a nearly linear increase with increasing nominal H(D) content, the volume expansion being about $1.1 \text{ \AA}^3/\text{H(D) atom}$. It should be noted that for the samples containing H(D), the values of the lattice parameter determined from the neutron diffraction measurements are somewhat higher than those derived from X-ray diffraction (see Section 2). The fraction of the minor TiCo phase with CsCl-type structure tends to increase with increasing H(D) content. This indicates that the reaction of Ti_2Co with hydrogen leads to a partial disproportionation [23,24]. Since the lattice parameter of the TiCo phase in all four samples is nearly the same, we can conclude that this phase does not contain hydrogen. The neutron diffraction pattern for $\text{Ti}_2\text{CoD}_{1.0}$ exhibits an additional set of broad lines corresponding to a small amount of a finely dispersed TiD_2 phase with CaF_2 -type structure. This phase is clearly the product of a partial disproportionation. Note that the presence of this phase has not been revealed by X-ray diffraction measurements.

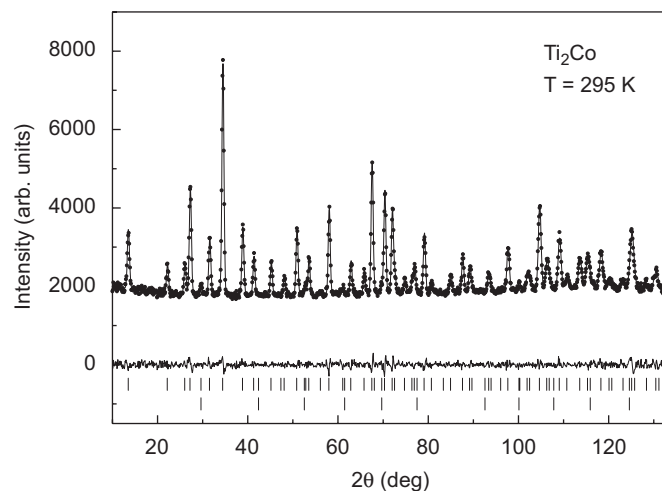


Fig. 5. Observed (circles) and calculated (solid line) neutron diffraction patterns for Ti_2Co at 295 K. The solid line below the data shows the difference between the observed and calculated diffraction patterns. Vertical bars indicate the calculated positions of Bragg peaks for Ti_2Co (top) and TiCo (bottom) phases.

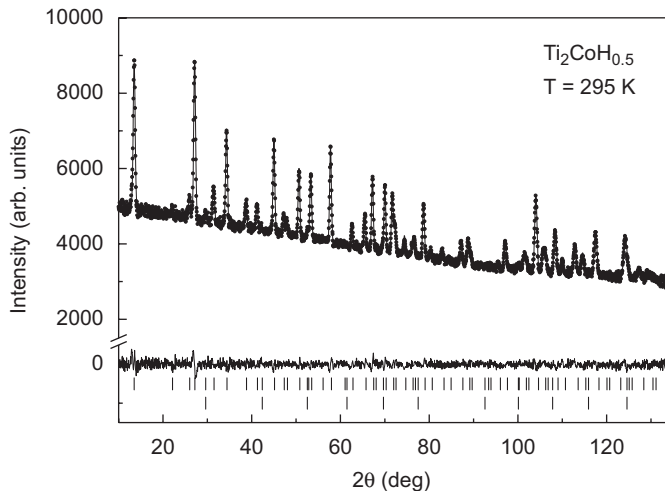


Fig. 6. Observed (circles) and calculated (solid line) neutron diffraction patterns for $\text{Ti}_2\text{CoH}_{0.5}$ at 295 K. The solid line below the data shows the difference between the observed and calculated diffraction patterns. Vertical bars indicate the calculated positions of Bragg peaks for Ti_2CoH_x (top) and TiCo (bottom) phases.

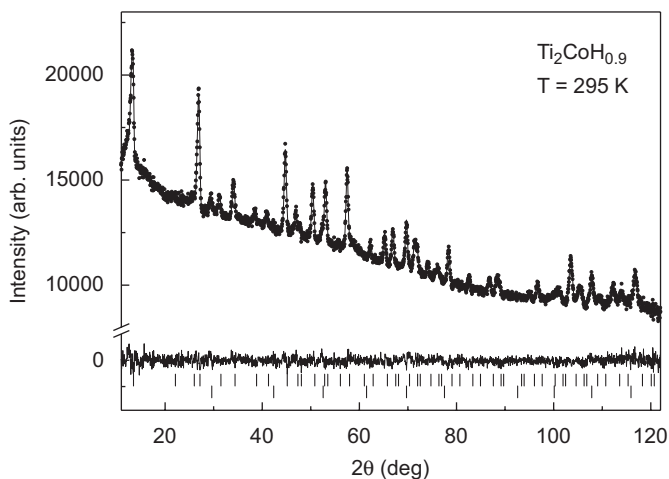


Fig. 7. Observed (circles) and calculated (solid line) neutron diffraction patterns for $\text{Ti}_2\text{CoH}_{0.9}$ at 295 K. The solid line below the data shows the difference between the observed and calculated diffraction patterns. Vertical bars indicate the calculated positions of Bragg peaks for Ti_2CoH_x (top) and TiCo (bottom) phases.

The structural parameters and the agreement factors resulting from the fits to the neutron diffraction data for $\text{Ti}_2\text{CoH}_x(\text{D}_x)$ are listed in Table 1. In order to reduce the number of fit parameters, we have assumed that the isotropic temperature factors are common for atoms of the same type in different positions. For the hydrogen-free Ti_2Co , we have found that the fit is essentially improved when a small part of Ti atoms substitute for Co in the Co sublattice. This is consistent with the presence of the Ti-poor TiCo phase. Therefore, the possibility of a partial Ti substitution in the Co sublattice has been considered for all the samples studied, and the occupancy of the Co sublattice by Co atoms has been a variable parameter in the fits. As potential H(D) sites, we have considered all 6 tetrahedral

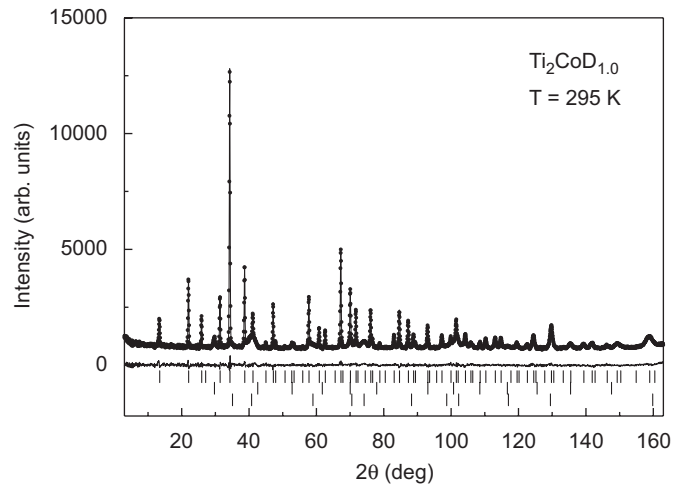


Fig. 8. Observed (circles) and calculated (solid line) neutron diffraction patterns for $\text{Ti}_2\text{CoD}_{1.0}$ at 295 K. The solid line below the data shows the difference between the observed and calculated diffraction patterns. Vertical bars indicate the calculated positions of Bragg peaks for Ti_2CoD_x , TiCo and TiD_2 (from the top).

and two octahedral interstices specified in Section 3.2. The starting positional parameters of H(D) atoms at these sites are taken from the analysis of Westlake [22]. In $\text{Ti}_2\text{CoH}_{0.5}$, only octahedral 16c and 8a sites are found to be occupied by H atoms. The occupancy of both these sites exceeds one-half. In $\text{Ti}_2\text{CoH}_{0.9}$ and $\text{Ti}_2\text{CoD}_{1.0}$, in addition to nearly completely filled octahedral 16c and 8a sites, the tetrahedral 96g₁ and 96g₂ sites are found to be partially occupied by H(D) atoms. The addition of H(D) atoms at the other tetrahedral sites does not improve the fits. The positional parameters of H(D) atoms at 96g₁ and 96g₂ sites (Table 1) appear to be close to those calculated for Ti_2NiH_x on the basis of the geometric model [22,25]. It should be noted that a partial occupation of 96g₁ sites was also reported for Ti_2Ni -type deuterides Hf_2FeD_x ($x = 3, 4$ and 5) [3] and for oxygen-stabilized Ti_2Ni -type systems $\text{Ti}_4\text{Fe}_2\text{OD}_{2.25}$ [26] and $\text{Zr}_3\text{V}_3\text{OD}_{4.93}$ [27], and a partial occupation of 96g₂ sites was found for Hf_2FeD_4 , Hf_2FeD_5 [3] and $\text{Zr}_3\text{V}_3\text{OD}_{4.93}$ [27]. For $\text{Ti}_2\text{CoH}_{0.5}$ and $\text{Ti}_2\text{CoH}_{0.9}$ the refined hydrogen content (0.46 and 0.85 H atoms/formula unit, respectively) is in reasonable agreement with that determined from hydrogen absorption. However, for $\text{Ti}_2\text{CoD}_{1.0}$ the refined D content in the dominant phase (0.78 D atoms/formula unit) is considerably lower than that derived from the absorption. This discrepancy may be attributed (at least, partially) to the presence of the minor TiD_2 phase with high D concentration.

In order to discuss possible paths of hydrogen jump motion in $\text{Ti}_2\text{CoH}_x(\text{D}_x)$, we have to consider the distances between the sites partially occupied by H(D) atoms. The distances (shorter than 2.5 Å) within the deuterium sublattice for $\text{Ti}_2\text{CoD}_{1.0}$ are listed in Table 2. The octahedral sites 16c and 8a form a network through which long-range diffusion can occur. This is consistent with the fact that both 16c and 8a sites are occupied at low H(D)

Table 1
Structural parameters for $\text{Ti}_2\text{CoH}_x(\text{D}_x)$ resulting from profile refinements^a

Atom	Position	Parameter	Ti_2Co	$\text{Ti}_2\text{CoH}_{0.5}$	$\text{Ti}_2\text{CoH}_{0.9}$	$\text{Ti}_2\text{CoD}_{1.0}$
Ti1	48f ($x, 1/8, 1/8$)	$a_{\text{Ti}_2\text{Co}}$ (Å)	11.2881(4)	11.3370(3)	11.3678(7)	11.3789(2)
		x	0.9364(2)	0.9334(2)	0.9321(3)	0.9332(2)
		n	1	1	1	1
		B (Å ²)	0.62(3)	0.84(3)	1.04(6)	1.08(4)
Ti2	16d ($1/2, 1/2, 1/2$)	n	1	1	1	1
		B (Å ²)	0.62(3)	0.84(3)	1.04(6)	1.08(4)
Co	32e (x, x, x)	x	0.2858(2)	0.2863(2)	0.2865(3)	0.2865(2)
		n	0.970(1)	0.981(5)	0.955(8)	0.970(1)
		B (Å ²)	0.59(8)	1.01(9)	0.9(2)	1.05(7)
H1(D1)	16c (0,0,0)	n		0.586(8)	0.85(1)	0.912(6)
		B (Å ²)		2.1(1)	1.8(1)	1.68(3)
H2(D2)	8a ($1/8, 1/8, 1/8$)	n		0.66(1)	0.84(2)	0.912(8)
		B (Å ²)		2.1(1)	1.8(1)	1.68(3)
H3(D3)	96g ₁ (x, x, z)	x			0.797(3)	0.783(1)
		z			0.169(5)	0.152(1)
		n			0.040(5)	0.020(2)
		B (Å ²)			1.8(1)	1.68(3)
H4(D4)	96g ₂ (x, x, z)	x			0.864(6)	0.860(1)
		z			0.518(4)	0.520(1)
		n			0.032(4)	0.012(1)
		B (Å ²)			1.8(1)	1.68(3)
		$\Sigma\text{H(D)}$		0.46	0.85	0.78
		a_{TiCo} (Å)	2.9974(9)	2.998(1)	2.9955(6)	3.0008(6)
		F_{TiCo} (wt%)	1.9(2)	2.0(2)	4.7(3)	11.8(6)
		a_{TiD_2} (Å)				4.425(1)
		F_{TiD_2} (wt%)				4.7(1)
		R_{wp} (%)	3.02	1.80	1.22	4.08
R_{p} (%)	2.37	1.42	0.95	3.17		
χ^2	1.97	1.34	1.76	1.56		

^aSpace group of the dominant phase: $\text{Fd}\bar{3}\text{m}$, the origin is at $\bar{3}\text{m}$. a_x is the lattice parameter, n the site occupancy factor, B_x the isotropic temperature factor, $\Sigma\text{H(D)}$ the total number of H(D) atoms (per formula unit) in the dominant phase and F_x the fraction of a minor phase. R_{wp} , R_{p} and χ^2 are the standard agreement factors. Calculated standard deviations for the last digit of parameters are given in parentheses.

Table 2
The distances (in Å) between the interstitial sites partially occupied by D atoms in $\text{Ti}_2\text{CoD}_{1.0}$

Interstitial sites	16c	8a	96g ₁	96g ₂
16c	—	2.46 (2)	1.81 (6)	—
8a	2.46 (4)	—	—	—
96g ₁	1.81 (1)	—	2.06 (2), 2.11 (2)	1.74 (2)
96g ₂	—	—	1.74 (2)	0.48 (1), 2.09 (2), 2.37 (4)

Only the distances shorter than 2.5 Å are shown. The number of the neighbors at the same distance is shown in parentheses. The table is read horizontally, e.g., the 16c site has 6 nearest-neighbor 96g₁ sites at a distance of 1.81 Å.

concentrations. However, the distance between the nearest-neighbor 16c and 8a sites is rather large (2.46 Å), so that the exclusive filling of the octahedral sites is expected to result in low hydrogen mobility, in agreement with the R_1 data for $\text{Ti}_2\text{CoH}_{0.5}$ (Section 3.1). The tetrahedral 96g₁ sites are the nearest neighbors of 16c sites. As can be seen from Table 2, a partial filling of 96g₁ sites introduces shorter distances in the sublattice of sites available for hydrogen

(1.81 Å for 16c–96g₁ and 2.06 Å for 96g₁–96g₁). This is likely to result in an increase in hydrogen mobility. The tetrahedral 96g₂ sites are well separated from the octahedral 16c and 8a sites, so that hydrogen atoms can reach the sublattice 96g₂ sites only via short 96g₁–96g₂ contacts. The interesting feature of the sublattice of 96g₂ sites is that it consists of pairs of sites with the nearest-neighbor distance as small as 0.48 Å. It is tempting to ascribe the fast jump

process in $\text{Ti}_2\text{CoH}_x(\text{D}_x)$ to localized motion of H(D) atoms within such pairs of sites. However, the jump rate for a localized H(D) motion with such a small jump length is expected to be much higher than that found in our R_1 measurements for $\text{Ti}_2\text{CoH}_x(\text{D}_x)$ with $x \geq 0.9$ (the distance between sites is comparable to the hydrogen vibration amplitude). Furthermore, instead of moving between two closely spaced $96g_2$ through a common trigonal face of two adjacent Ti_2Co_2 tetrahedra, a hydrogen atom may reside at the center of this face (at the 48f site with Ti_3Co_2 coordination). The occupation of 48f sites cannot be distinguished from that of $96g_2$ sites on the basis of analysis of neutron diffraction patterns.

The location of H(D) atoms in $\text{Ti}_2\text{CoH}_x(\text{D}_x)$ with $x \approx 1$ suggests the following picture of H(D) diffusion in these compounds. Most of H(D) atoms occupy the nearly completely filled sublattice of octahedral (16c and 8a) sites. In addition to direct 16c–8a jumps, hydrogen atoms can jump to the nearest tetrahedral sites via short 16c– $96g_1$ contacts. The sublattice of tetrahedral ($96g_1$ and $96g_2$) sites is characterized by rather short nearest-neighbor distances and a low degree of H(D) filling. Therefore, a hydrogen atom can easily move on the sublattice of tetrahedral sites; it is expected to perform a number of jumps on this sublattice before it finds a vacant octahedral site. Thus, the fast H(D) motional process in $\text{Ti}_2\text{CoH}_x(\text{D}_x)$ with $x \approx 1$ may be attributed to the jump motion on the sublattice of tetrahedral sites. The details of this motion could be clarified by quasielastic neutron scattering experiments. Such experiments are in progress.

4. Conclusions

The analysis of our inelastic neutron scattering and neutron diffraction data for $\text{Ti}_2\text{CoH}_x(\text{D}_x)$ has shown that in $\text{Ti}_2\text{CoH}_{0.5}$, hydrogen atoms occupy only the octahedral (16c and 8a) interstices with Ti_6 coordination. As the hydrogen concentration in $\text{Ti}_2\text{CoH}_x(\text{D}_x)$ changes from $x = 0.5$ to $x \approx 1$, the sublattice of the octahedral sites appears to be nearly completely filled, and H(D) atoms start to occupy the tetrahedral $96g_1$ (Ti_3Co) and $96g_2$ (Ti_2Co_2) sites. The partial occupancy of the tetrahedral sites gives rise to the fast H(D) motion with the characteristic jump rate of about $3 \times 10^8 \text{ s}^{-1}$ at room temperature. Additional experiments are required to elucidate the mechanism of this fast motion.

Acknowledgments

This work was supported by the Russian Foundation for Basic Research (Grant no. 06-02-16246) and by the Priority

Program “Basic Energy Problems” of the Russian Academy of Sciences. A.V. Skripov also acknowledges financial support from the NIST Center for Neutron Research.

References

- [1] H. Buchner, M.A. Gutjahr, K.D. Beccu, H. Säuferer, *Z. Metallk.* 63 (1972) 497.
- [2] K.H.J. Buschow, A.M. van Diepen, *Solid State Commun.* 31 (1979) 469.
- [3] J.L. Soubeyroux, D. Fruchart, S. Derdour, P. Vuillet, A. Rouault, *J. Less-Common Met.* 129 (1987) 187.
- [4] J. Töpler, E. Lebsanft, R. Schätzler, *J. Phys. F* 8 (1978) L25.
- [5] T.C. Jones, T.K. Halstead, K.H.J. Buschow, *J. Less-Common Met.* 73 (1980) 209.
- [6] J.S. Cantrell, R.C. Bowman, A.J. Maeland, *J. Alloys Compounds* 330–332 (2002) 191.
- [7] A.L. Buzlukov, A.V. Skripov, A.V. Soloninin, V.N. Kozhanov, A.P. Stepanov, *J. Alloys Compounds* 352 (2003) 66.
- [8] A.L. Buzlukov, A.V. Soloninin, A.V. Skripov, *Solid State Commun.* 129 (2004) 315.
- [9] R.G. Barnes, in: H. Wipf (Ed.), *Hydrogen in Metals III*, Springer, Berlin, 1997, p. 93.
- [10] T.J. Udovic, D.A. Neumann, J. Leao, C.M. Brown, *Nucl. Instr. and Meth. A* 517 (2004) 189.
- [11] B.N. Goshchitskii, A.Z. Menshikov, *Neutron News* 7 (1996) 12.
- [12] J.K. Stalick, E. Prince, A. Santoro, I.G. Schroder, J.J. Rush, in: D.A. Neumann, T.P. Russel, B.J. Wuensch (Eds.), *Neutron Scattering in Materials Science II*, Materials Research Society, Pittsburgh, PA, 1995, p. 101.
- [13] J. Rodriguez-Carvajal, *Physica B* 192 (1993) 55.
- [14] L.R. Lichty, J.W. Han, R. Ibanez-Meier, D.R. Torgeson, R.G. Barnes, E.F.W. Seymour, C.A. Sholl, *Phys. Rev. B* 39 (1989) 2012.
- [15] A.V. Skripov, S.V. Rychkova, M.Yu. Belyaev, A.P. Stepanov, *J. Phys.: Condens. Matter* 2 (1990) 7195.
- [16] N.F. Berk, J.J. Rush, T.J. Udovic, I.S. Anderson, *J. Less-Common Met.* 172–174 (1991) 496.
- [17] A.V. Skripov, J.C. Cook, D.S. Sibirtsev, C. Karmonik, R. Hempelmann, *J. Phys.: Condens. Matter* 10 (1998) 1787.
- [18] A.V. Skripov, A.V. Soloninin, A.P. Stepanov, V.N. Kozhanov, *J. Phys.: Condens. Matter* 11 (1999) 10393.
- [19] A.L. Buzlukov, A.V. Skripov, *J. Alloys Compounds* 366 (2004) 61.
- [20] A.V. Skripov, A.V. Soloninin, V.N. Kozhanov, *Solid State Commun.* 122 (2002) 497.
- [21] A. Abragam, *The Principles of Nuclear Magnetism*, Clarendon Press, Oxford, 1961.
- [22] D.G. Westlake, *J. Less-Common Met.* 105 (1985) 69.
- [23] M.H. Mintz, Z. Hadari, M.P. Dariel, *J. Less-Common Met.* 74 (1980) 287.
- [24] A.J. Maeland, *J. Less-Common Met.* 89 (1983) 173.
- [25] H.W. Brinks, A.J. Maeland, B.C. Hauback, R.C. Bowman, J.S. Cantrell, *J. Alloys Compounds* 361 (2003) 108.
- [26] C. Stiou, D. Fruchart, A. Rouault, R. Fruchart, E. Raudaut, J. Rebière, *Mater. Res. Bull.* 16 (1981) 869.
- [27] F.J. Rotella, H.E. Flotow, D.M. Gruen, J.D. Jorgensen, *J. Chem. Phys.* 79 (1983) 4522.